Integrated Optic Tunable Add–Drop Filters for WDM Ring Networks

Salvatore Rotolo, Alberto Tanzi, *Member, IEEE*, Stefano Brunazzi, Domenico DiMola, *Member, IEEE*, Lucio Cibinetto, Maurizio Lenzi, *Member, IEEE*, *Member, OSA*, Gian-Luca Bona, Bert Jan Offrein, Folkert Horst, Roland Germann, Huub W. M. Salemink, and Peter H. Baechtold

***Abstract*—This paper deals with two types of thermo-optically tunable add–drop filters realized by means of different technologies: fiber-matched low-pressure chemical vapor deposited (LPCVD)-grown SiO_2 waveguides and plasma-enhanced chemical vapor deposition (PECVD)-grown high-refractive-index-contrast SiON waveguides. Design and technology aspects are outlined. The device characterizations, drawn from laboratory and field trial measurements, are reported. The description focuses on the device applications in a system context. In particular, the usefulness of the components as the basic elements of an optical add–drop multiplexer node, suitable for a ring network, is shown. The key component aspects are presented as strictly related to system requirements and issues.**

***Index Terms*—Add–drop, bit-error rate (BER), integrated optics, ring network, tunable, wavelength-division multiplexing (WDM).**

I. Introduction

OPTICAL networks are becoming a reality as the physical layer of high-performance telecommunication networks. The deployment of wavelength-division multiplexing (WDM) technology allows the full exploitation of the already installed fibers now facing an increasing traffic capacity demand. The routing of channels at the optical level and the insertion/extraction of channels in/from WDM aggregates, without preventing the transparent transit of throughput traffic, are key functions to ensure networking capabilities, support advanced protection and restoration schemes, and deploy a general-purpose platform for several types of clients. [1]–[3].

The functionality ascribed to the optical layer might be performed in the client layer after demultiplexing in both wavelength and time domains. This requires, however, that the electronic equipment is sized according to the total channel throughput at each node, rather than according to the terminated traffic, causing a marked cost increase. On the other hand, photonic systems may be costly in themselves. The best tradeoff between optical and electrical functionality depends on the application environment.

Manuscript received July 19, 1999; revised December 27, 1999. This work was supported in part by the European Research Program ACTS and has been carried out in the framework of the AC069 COBNET project.

S. Rotolo, A. Tanzi, S. Brunazzi, D. DiMola, L. Cibinetto, and M. Lenzi are with the R&D Department, Italtel Photonic Unit, Milan 20019, Italy.

G. L. Bona, B. J. Offrein, F. Horst, R. Germann, H. W. M. Salemink, and P. Baechtold are with IBM Research Division, Zurich Research Laboratory, Rüschlikon 8803, Switzerland.

Publisher Item Identifier S 0733-8724(00)03041-3.

In this paper, a local area network scenario [metropolitan area network (MAN), local area network (LAN), corporate network] is considered. A ring topology is suitable in this context because it offers simple and efficient protection schemes [4]. A typical corporate-network fiber ring spans some tens of kilometers, is designed to connect several nodes (up to 10–12), making a high bit-rate channel (up to 2.5 Gb/s) available to each one, and can be tailored to different traffic types (adjacent, hub, uniform). The requirements for this scenario are sufficient to justify the application of WDM techniques to transmission and routing tasks, but the use of nodes based on a complete WDM demultiplexing and multiplexing would be critical in terms of cost. The availability of low-cost nodes, without forgoing the performance enhancement enabled by photonic technology, is very important. In the proposed configuration, hub traffic is supposed. So, one node plays the role of hub, which is to switch at electronic level the traffic directed to each of the other ring nodes and the traffic to/from other networks.

The other ring nodes are optical add–drop multiplexers (OADM). The bidirectional communication between each OADM and the hub node is achieved by locally extracting, terminating, and reinserting the wavelengths related to the OADM itself, allowing the other wavelengths to cross the node transparently. The distinction between terminated and throughput traffic, therefore, is done at the optical level. The key functions of an OADM node can be performed by one optical add–drop filter (ADF), thus achieving significant cost advantages.

In this paper, two versions of ADF suitable for this use are presented. A functional description of the ADF is reported in Section II; the design approach is outlined in Section III; the two components realized are described in Sections IV and V; details about the pigtailing procedure are given in Section VI. Then attention is focused in Section VII on a system-level characterization, based on the results obtained from the trial network for which the components were realized, the field demonstrator developed in the European Project ACTS COBNET (corporate optical backbone network).

II. Functional Description of the Add–Drop Filter

A. System Context

The test network considered is outlined in Fig. 1. The hub node, called "HE" (high end), includes an electronic space switch, a set of optical transmitters (HE Tx) and receivers (HE Rx), and WDM multiplexers/demultiplexers (Mux/Demux).

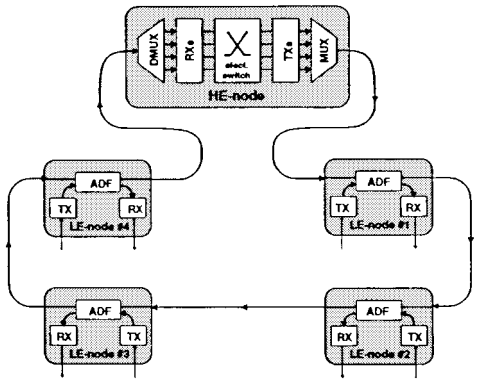

Fig. 1. Scheme of the corporate-network ring. Actually, a two-fiber ring characterized by equipment redundancy and fiber duplication (not shown in the figure) was implemented for protection purposes.

The OADM's along the ring, defined as "LE" (low ends), are based on the ADF device, and also include a transmitter (LE Tx) and a receiver (LE Rx). The ring is composed of N nodes ($N = 4$ in Fig. 1). If a one-to-one wavelength/node correspondence is assumed, a WDM signal composed of $N = 4$ wavelengths travels along the ring; the ith LE node extracts and terminates, generates and transmits the ith wavelength.

Given a wavelength, its "downstream" path in the ring (from HE to LE) transports information to be received by a LE node, whereas its "upstream" path (from LE to HE) carries the information transmitted by a LE node. At the HE node each channel is routed to the proper LE node: The corresponding received data stream is switched spatially in the electronic domain to the transmitter whose wavelength is associated with the destination LE node. In this sense, the ring supports a wavelength-based routing scheme.

B. System Requirements

The main system issues identified in the considered ring network are discussed in this section.

1) The system power budget must ensure that the optical channel power, before any Rx of any node, is larger than the Rx sensitivity, keeping a sufficient power margin to counteract other causes of transmission degradation. Power levels at the boundaries of the optical paths are limited by the features of the Tx and Rx available at low cost. Thus, the power budget directly imposes the maximum acceptable loss in the ring optical paths and, indirectly, the tolerable ADF insertion losses. These requirements can be relaxed if optical amplifiers are used along the ring, but this choice would increase costs. The power budget has to be tailored to the worst-case optical path, covering N links, passing through N nodes. The operating conditions for the other optical paths are actually better. Power equalization of WDM channels is not guaranteed: This fact, acceptable by itself, can cause impairments related to the optical crosstalk.
2) Optical crosstalk acts in the ring as a manifold cause of performance degradation. HE Rx are mainly affected by the interference generated by the HE Demux, LE Rx by the crosstalk generated in the ADF. Crosstalk can be classified as homo-wavelength or hetero-wavelength, according to whether the interfering and received channels are at the same wavelength or not. Crosstalk can also have different degrees of coherence: it is "completely coherent" when the central wavelength, the carrier phase, and the modulating bit pattern of the interfering and received signals are perfectly matched; it is "completely noncoherent" when all these variables are uncorrelated. Hybrid situations between the two extremes may occur. The "partially coherent" homo-wavelength crosstalk, arising in the ADF from the interference of the added channel on the dropped one, is a very detrimental effect. A system countermeasure implies the reduction of the transmitted power at the LE node, consistent with the power budget. The disadvantage of this method is the necessity to control the transmitted power level. The countermeasures on the component are: a) the improvement of the crosstalk isolation of the device and b) an alternative design based on the add-after-drop structure discussed in Section V.
3) The transparency for optical paths along the ring requires that the degradation due to the cascade of N optical nodes be minimized. This could be critical for OADM's requiring the full demultiplexing of the WDM signal: the cascade of selective spectral functions traversed by each channel (two times at each crossed node) emphasizes the end-to-end spectral bandwidth narrowing. From this perspective, the proposed ADF-based OADM is advantageous because it allows the transparent transit at the aggregate level of the throughput channels. In this case, each channel passes through only two selective windows ("add" and "drop").
4) The relative wavelength precision among lasers, ADF spectral functions, and selective Mux/Demux spectral windows is essential to avoid additional losses and to reduce signal distortions. Therefore, the availability of tunable ADF is of interest to allow a fine system setting. The drop response can be finely tuned to the wavelength to be received, and the transmitter laser can be adjusted accordingly; hence, a local optimization can be achieved at each LE node.
5) Tunability over the entire WDM spectral range is not strictly required. This function is useful, however, to allow the system upgrade toward wavelength reconfigurable rings; in this case, a common design for all the ADF's to be used in different OADM's can be exploited.
6) The system must work on lightwaves of an uncontrolled, time-varying polarization state. Consequently, the components must guarantee acceptable performance (loss, crosstalk, spectral response) for any polarization of the input light. This can be achieved by minimizing the polarization dependence of ADF parameters or by tracking the slow variations of the input light polarization to exploit the device tunability. The latter option has the disadvantage of requiring a complex control loop.

It should be recalled that the discussed requirements are dictated by a context where: a) a one-to-one wavelength/node correspondence and b) a fixed node/wavelength association—are

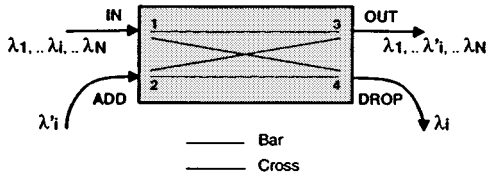

Fig. 2. ADF functional scheme.

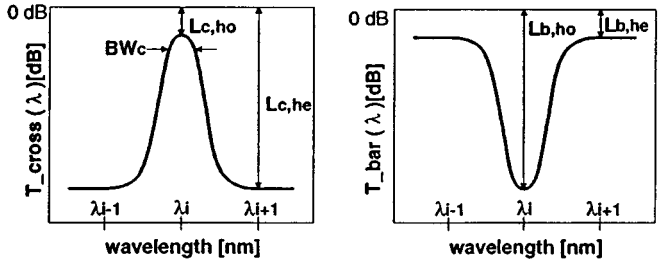

Fig. 3. CROSS and BAR spectral functions of the ADF.

assumed. This scenario is considered as a significant reference, in this paper. The use of the ADF, indeed, can be extended to other applications.

The capability of dropping two or more wavelengths in a node can be obtained by cascading two or more filters in that node. The possibility of sharing a wavelength among different nodes can be achieved through a proper OADM design, i.e., by offering the so-called "drop and continue" function (e.g., by combining optical splitting and selective add–drop function). In both cases, the optical power-budget of the ring should be obviously redefined.

Moreover, the property of ring reconfigurability is already in principle enabled by the wide-range tunability of the proposed ADF component. This includes the possibility of adding one or more nodes in the ring, provided that the new wavelengths assigned to the new nodes, besides respecting the agreed wavelength grid, lie inside the free spectral range of the ADF spectral response (see Section III).

C. Functional Description of ADF

The items listed above have a direct impact on component design and functionality. The ADF is sketched in Fig. 2 as a four-port unidirectional black-box device.

A transmission matrix $T(\lambda)$, whose elements are the transmission parameters, can be defined

$$\text{In to Drop: } T_{14}(\lambda), \quad \text{Add to Out: } T_{23}(\lambda)$$
$$\text{In to Out: } T_{13}(\lambda), \quad \text{Add to Drop: } T_{24}(\lambda).$$

If a symmetric transmission matrix is considered, the four parameters reduce to only two: $T_{14} = T_{23} = T_{\text{cross}}$; $T_{13} = T_{24} = T_{\text{bar}}$. Actually, these parameters are spectral functions, whose qualitative shapes are sketched in Fig. 3. The "cross" function has a passband-selective shape to add and drop the channel at λ_i and filter out the other ones at λ_{i-1}, λ_{i+1}, etc. The "bar" function has a notch shape to extract the channel at λ_i and to let the other channels pass through.

In Fig. 3, the following insertion loss and filter bandwidth parameters can be identified:

$L_{c,\,ho}$ Cross homo-wavelength loss (at $\lambda = \lambda_i$).
$L_{c,\,he}$ Cross hetero-wavelength loss (min. loss at $\lambda_k \neq \lambda_i$).
$L_{b,\,ho}$ Bar homo-wavelength loss (at $\lambda = \lambda_i$).
$L_{b,\,he}$ Bar hetero-wavelength loss (max. loss at $\lambda_k \neq \lambda_i$).
BW_c Cross bandwidth.

Significant parameters, from the perspective of system requirements, can be derived from the previous definitions

$L_{\text{drop}} = L_{\text{add}} = L_{c,\,ho}$ Insertion loss for the channel that is extracted or inserted (drop or add loss).
$L_{\text{through}} = L_{b,\,he}$ Insertion loss for the channels that pass through (through loss).
$X_{ho} = (L_{b,\,ho})/(L_{c,\,ho})$ Homo-wavelength crosstalk isolation.
$X_{he} = (L_{c,\,he})/(L_{c,\,ho})$ Hetero-wavelength crosstalk isolation.

Definitions are provided for linear values. However, logarithmic parameter values and figure scales will be often used, throughout the paper. According to the adopted convention, logarithmic loss and crosstalk are positive.

Regarding the loss parameters, it can be noted that the through loss is particularly critical, because it is experienced by each channel several times (up to $N-1$ times) along the ring, whereas add and drop losses are to be counted only once. An estimation based on typical power-budget assumptions leads us to require $L_{\text{through}} < 4$ dB and <2 dB, for 4 and 8-node rings, respectively. The realization of rings with a larger number of nodes seems to be possible only through the use of optical amplifiers.

The crosstalk parameters warrant some further remarks. X_{ho} is related to the interference of the not completely suppressed fraction of the added signal on the dropped channel, causing homo-wavelength crosstalk at the LE Rx. It also represents the interference of the residual fraction of the dropped signal on the added channel, causing homo-wavelength crosstalk at the remote HE Rx. Let us focus on the crosstalk at LE Rx. The actual interference strength must be evaluated in terms of the power imbalance between the interfering channels. A further parameter is therefore defined, namely the signal-to-homo-wavelength-crosstalk ratio at the LE Rx:

$$\text{SCR}_{ho} = (X_{ho})/(\Delta P_{ho}), \tag{1}$$

where $\Delta P_{ho} = [P_{\text{add}}(\lambda_i')]/[P_{\text{in}}(\lambda_i)]$. The value of ΔP_{ho}, expressed in dB, is usually positive and tends to worsen the effective SCR_{ho}. The homo-wavelength crosstalk can be counteracted at the component level by improving X_{ho} at the system level by reducing ΔP_{ho}, e.g., by lowering the transmitted power.

X_{he} is related to the interference of the residual fractions of the through channels on the dropped signal, causing hetero-wavelength crosstalk at the LE Rx. A further parameter, the signal-to-hetero-wavelength-crosstalk ratio, is necessary to evaluate the actual impact of this type of crosstalk, depending on the number and power levels of the WDM channels

$$\text{SCR}_{he} = (X_{he})/(\Delta P_{he}) \tag{2}$$

where $\Delta P_{he} = [\Sigma P_{\text{in}}(\lambda_k)]/[P_{\text{in}}(\lambda_i)]$, $k \neq i$. ΔP_{he} is the ratio between the overall power of the through channels and the power of the dropped channel at the "IN" port of the ADF. The value of ΔP_{he}, expressed in dB, is generally positive.

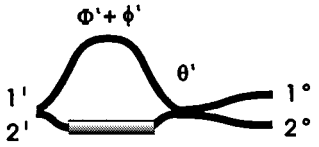

Fig. 4. Basic element for the ADF, composed of one optical delay line, an optical directional coupler and a thermo-optical heater phase shifter.

It should be remarked that (1) and (2) are expressions of linear quantities, but logarithmic parameter values will be usually adopted in the following sections.

A "qualitative" bandwidth parameter, BW_c, is introduced in Fig. 3. BW_c, measured at -1 dB, is related to the flatness of the add and drop spectral responses, which should be maximized to reduce signal distortion. Values larger than 0.4 nm are acceptable for bit rates up to 2.5 Gb/s.

III. Add–Drop Filter Design

Various approaches have been shown to implement optical add–drop filters. Fiber Bragg grating devices, either with circulators or in a Mach–Zehnder interferometer configuration, show excellent optical characteristics such as low insertion losses and high channel isolation [5]. This also holds for hybrid components based on dielectric filter plates. However, tuning of fiber gratings and dielectric filters is not trivial, and in order to enhance the functionality of WDM networks further dynamic reconfigurability is an important item, as noted in Section II-B. Tunable add–drop components based on the acousto-optic effect, for example in lithium niobate [6], [7], exhibit good and flexible filter characteristics, but the materials involved and the requirement of an RF generator make this approach relatively expensive. As a more cost-effective alternative, glass-type planar waveguide filters can be made tunable by using the thermooptic effect. Both types of tunable add–drop filters described in this paper are based on the resonant coupler (RC) principle [8], a cascade of multiple stages, each one based on a directional coupler, and an optical delay line as shown in Fig. 4.

A typical feature of these filters is the periodicity of their transmission functions. The free spectral range (FSR) parameter, defined as the spectral interval between two adjacent periodic peaks, is subject to the constraint of being larger than the entire range of the WDM signal handled.

The optical delay line consists of a unit length, which is the same for all the stages and determines the FSR, plus a phase shifter (between $-\pi$ and $+\pi$) that may differ for every stage. Tuning is achieved by changing the effective refractive index in the delay line arms. As the absolute arm lengths are of the order of a few millimeters, a small effective refractive index change in one of the arms suffices to effect a 2π phase shift, allowing the device to be tuned over a complete FSR. If the typical value of the glass thermo-optic coefficient is considered ($\Delta n/\Delta T = 10^{-5}\ \mathrm{K}^{-1}$), a 3-mm heating length requires a local temperature increase of 50 K.

The transmission matrix of the basic stage is expressed in (3), where Θ^i is the ith coupling angle, $\Phi + \phi^i$ is the ith phase shift due to the unequal arm lengths, and $\Delta(T)$ is the phase shift due to the temperature difference (ΔT) between the two arms of the optical delay lines, controlled by a single heater

$$T^i = \begin{bmatrix} e\dfrac{-j(\Phi+\phi^i-\Delta(T))}{2} & 0 \\ 0 & e\dfrac{+j(\Phi+\phi^i-\Delta(T))}{2} \end{bmatrix} \cdot \begin{bmatrix} \cos\Theta^i & j\sin\Theta^i \\ j\sin\Theta^i & \cos\Theta^i \end{bmatrix}. \quad (3)$$

The overall transmission matrix, obtained from the product of the single-stage matrices, is the same as the one mentioned in Section II-C, apart from normalization coefficients. The required number of RC stages increases with the finesse of the drop response.

An example of an RC design technique based on the weighting of the directional couplers is reported in [8]. A more general design approach starts with the frequency response of the drop transfer of an RC with N stages described by the polynomial

$$F(z) = \sum_{k=0}^{N} b_k z^{-k} \quad (4)$$

where

z $= e^{j\omega\Delta\tau}$;
ω radial frequency;
$\Delta\tau$ unit delay in the delay line arms.

Note that $\omega\Delta\tau = \Phi$, (3). The complex coefficients b_k are the amplitudes of the harmonics with a periodicity of $\Delta\omega = 2\pi/k\Delta\tau$ and are derived from the desired transfer characteristics by using finite impulse response (FIR) design methods, as known from digital filter theory [9], [10]. The zeroes of the polynomial in (4) can be used for the design. Coupling ratios in the directional couplers and phase shifts in the delay lines can be related to the polynomial (4), as described in [9], [11].

IV. Description of Glass-on-Silicon ADF

The glass-on-silicon technology [12], by low-pressure chemical vapor deposition (LPCVD) of silica layers, has been adopted by the Italtel Photonic Unit to realize an ADF component. It is designed to add and drop one channel from a comb of four WDM channels spaced 3.2 nm apart, and it is suitable for use in the ring shown in Fig. 1. Tunability is ensured over the entire 12.8-nm FSR. The device is realized by cascading three basic elements, as shown in Fig. 5.

An appropriate selection of coupling ratios, delay lengths, and concentrate phase shifts, allows the "cross" response zeros to be allocated at the wavelengths of the through channels to optimize the hetero-wavelength crosstalk isolation on the dropped channel.

The control on the refractive index difference and the physical waveguide parameters allowed to reproduce the coupling lengths with a 1–5% accuracy in the measured devices.

The measured spectral responses of the device are shown in Fig. 6. The following values can be derived for the main parameters (defined in Section II-C): $L_{\mathrm{drop}} = L_{\mathrm{add}} = L_{\mathrm{through}} = 2$ dB, $X_{ho} > 13$ dB, $X_{he} > 16$ dB, BW_c (at -1 dB) $=2$ nm.

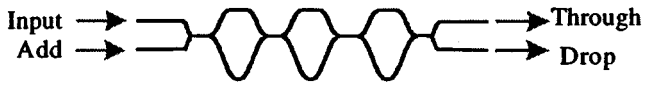

Fig. 5. Layout of the ADF structure.

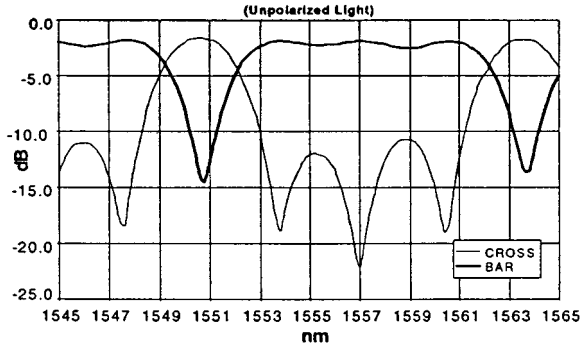

Fig. 6. Measured BAR and CROSS responses of the untuned ADF.

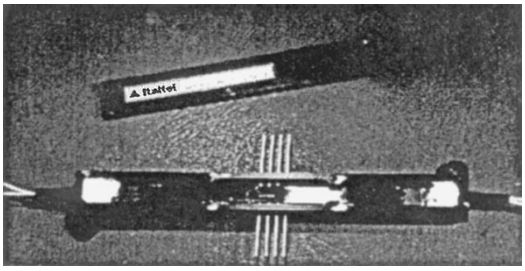

Fig. 7. LPCVD glass-on-silicon ADF device in package.

The obtained results are substantially consistent with the expected targets. Loss values are even slightly better than foreseen. The homo-wavelength crosstalk isolation is on the contrary slightly worse than the expected value (it is opportune to recall that measurements were performed in a worst case condition, i.e., on unpolarized light).

The device tuning on the entire FSR is demonstrated in [13]. The distortion of the spectral curves experienced after tuning is small. The parameter values reported above remain valid; the crosstalk isolation X_{ho} becomes even better (up to a 3-dB improvement).

The worst case filter tuning time (related to a reduction of the heater temperature, which is intrinsically slower than the correspondent temperature increase) is few ms.

The LPCVD (Fig. 7) fabrication of the planar waveguide device includes a steam oxidation of the silicon wafers, i.e., the deposition of a 15-μm undoped silica layer to form the buffer layer, the film annealing to relax the stress in the glass, and the deposition of the P glass (P-doped silica) core. The available technology allows us to grow up to 6 μm of this layer; the annealing helps to reorder the phosphorus atoms in the glass matrix, achieving the desired refractive index contrast and good uniformity. A reactive ion etching of the core layer patterns the waveguides. The last step is the coverage by an upper cladding by depositing an 18-μm layer of boron-phosphorous-doped silica. The presence of boron fluidizes the deposited film, ensuring good step coverage, and proper matching of the refractive index of the upper and lower claddings. The measured residual birefringence in the realized waveguide is low (less than 0.2 nm); the intrinsic loss of the straight waveguide is 0.03 dB/cm, so that the dominant loss mechanism is actually the fiber-waveguide coupling loss (about 0.5 dB/facet for a 4.8×5.5 μm^2 waveguide cross section).

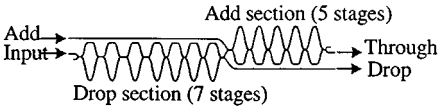

Fig. 8. Add-after-drop layout consisting of two resonant coupler devices.

Sputtering is used to realize the heater electrodes in nickel chromium alloy (60/40) [14]. This alloy guarantees high stability in a humid environment. Consequently, the package is not required to be hermetically sealed, thus reducing packaging costs. For the applications considered, the heater resistance ranges from 20 to 60 Ω, and the heater power dissipated on each stage for a shift along an entire FSR is around 1.2 W per stage.

The devices have been pigtailed with standard single-mode fibers by using silicon V blocks, and housed in aluminum packages, which act as heat sinks. During operation throughout the tuning range, the package temperature ranges from 45 to 60 °C.

V. Description of the SiON AADF

The ADF described in the previous section, pursued in the framework of the COBNET project, was the first one to be realized. Its characterization and testing provided experience that was exploited to realize the successive component versions. In particular, system-level evaluations suggested an add-after-drop filter (AADF) configuration to allow substantial performance enhancements.

In the IBM Research Division, a SiON-based waveguide technology was developed with an absolute index contrast of 3.3%, corresponding to an effective lateral index contrast of 0.02 [15]. The minimum achievable bending radius is 1.5 mm, i.e., one order of magnitude smaller than that of fiber-matched waveguides [16]. In order to keep these waveguides monomodal, the core dimensions have to be reduced to 2×3 μm^2. The increased fiber-to-chip coupling losses can be reduced to values of about 1 dB/facet by using lensed fibers, as shown in Section VI, or mode converters [17]. The SiON waveguide is grown onto a thermally oxidized silicon substrate by PECVD. After annealing the samples at 1140 °C, the waveguides are patterned by reactive ion etching. Subsequently the structure is covered with silicon-dioxide by PECVD. Chromium heater elements are deposited on the delay line arms of the RC devices.

Add–drop components were realized to select one wavelength channel from a comb of four, spaced 1.6 nm apart. The AADF design is shown in Fig. 8; all the stages necessary for the add-after-drop functionality have been cascaded in a single chip, thanks to the small bending radius of the waveguide structure.

The AADF approach allows the characteristics of the filter to be tailored to specific requirements, such as a flat passband for the drop response. On the whole, it can be stated that the AADF ensures good isolation performance: the separation of the add and drop functions eliminates homo-wavelength crosstalk at the

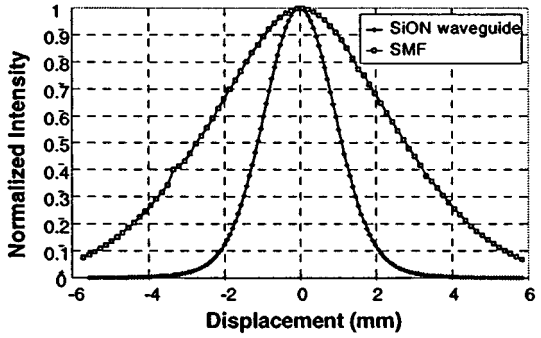

Fig. 9. Mode field distribution of SiON guide and standard SMF.

drop port (<-55 dB); the parameter X_{ho}, interpreted as the tail of the drop channel at the through port, is around 33 dB; the parameter X_{he} is better than 28 dB. On-chip through losses, due to both add and drop sections, were reported to be around 3.5 dB [16]. In order to reduce the expected penalty incurred by the device packaging, the pigtailing method has been improved as described in Section VI.

The tuning response time is well below 1 ms, which is smaller than for the ADF device realized in fiber-matched technology. This is caused by the smaller values of layer thickness used in SiON-technology and the corresponding better thermal contact to the silicon substrate.

Another valuable feature of the realized AADF is that each interferometric stage can be tuned individually, which allows the notch for each channel to be fine-tuned. More details on design goals and experimental results on the AADF can be found in [16] and [18].

In particular, the fabrication of the presented RC-structures is quite fault tolerant because of the individual heater tuning feature of the phase delay lines. Potential phase errors in the waveguides induced by process imperfections can be compensated. The process control of the directional couplers in SiON technology is realized to 1% accuracy of the coupling strength. This control together with the individual tuning feature results in a fabrication tolerant process for the RC-structures.

The delay line arm length difference sets the FSR of the RC device. Hence, smaller channel spacings can be obtained by simply increasing this length difference. The use of more wavelengths is possible by cascading more stages [19].

VI. Details of the SiON-AADF Pigtailing

The small dimensions of the mode field diameter of the SiON waveguide (see, Fig. 9) cause high insertion loss (>3.5 dB) in the coupling with a standard single mode fiber (SMF). This loss can be reduced by using a lensed fiber, but in this case the pigtailing procedure must be optimized in order to protect the lens. At Italtel Laboratories, a process is available that allows the lensing of the SMF pigtail by a chemically wet etching. The dimensions of the mode field diameter of the lensed fiber, which are dependent on the fiber etching time, can be matched to those of the waveguide by setting the proper process timing. In this way, a significant 2.5 dB/facet reduction of the coupling loss was achieved; consequently, the measured insertion loss of the pig-tailed component ranged from 7 dB (simple butt coupling) to 5 dB (lensed fiber for the output coupling), to 2.5 dB (lensed fiber at both sides).

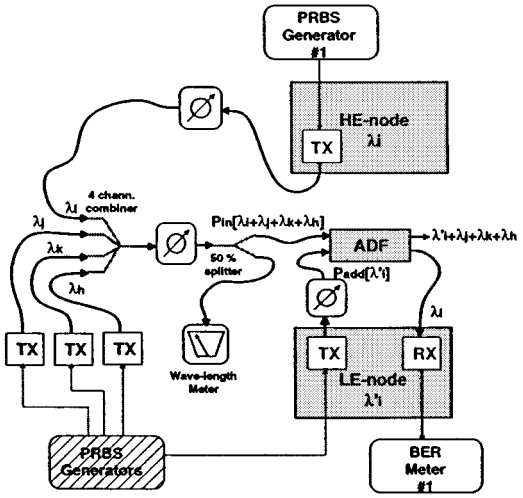

Fig. 10. Reference system test bench. The dropped (λ_i) and added (λ_i') channels are modulated at 622 Mb/s by two different PRBS words. Other interfering channels are modulated by different bit patterns and/or bit rates. The Rx sensitivity for BER$= 10^{-9}$ at 622 Mb/s is -30.5 dBm.

The pigtailing procedure is not easy for a lensed fiber because it must protect the lens and avoid the presence of glue between fiber and waveguide. An optimization can also be required for the lens position along the optical axis. In the available standard pigtailing scheme, a silicon V block, is used to glue the SMF to the chip; the same procedure is used to package the lensed fiber because the wet etching can also be done on a fiber mounted in a V block, without degrading the fiber or the V block. A silicon V block with two lateral epoxy dams has been employed to avoid the presence of glue in front of the lens. The approach described has been adopted for pigtailing the SiON-AADF device, obtaining an overall through loss of $L_{\text{through}} = 6$ dB. Add and Drop losses are in principle very similar to the through loss. Actual measured values were slightly higher ($L_{\text{add}} \sim L_{\text{drop}} \sim 7$ dB). An aluminum package placed on a copper heat sink with a thermo-optic cooler allowed an effective thermal dissipation.

VII. System-Level Characterization Measurements

The functionality of both kinds of filters has been evaluated by performing bit-error rate (BER) measurements in different system configurations. The reference laboratory test setup, simulating as much as possible a real working environment, is sketched in Fig. 10. Complete trial tests were then carried out during the COBNET network integration.

A. ADF Characterization

By using a proper setup of the test bench shown in Fig. 10, the ADF homo-wavelength crosstalk performances have been evaluated. The downstream channel λ_i is dropped and terminated. The upstream channel, at the same nominal wavelength λ_i', is inserted at the add port with different power levels. Other interfering channels are not present.

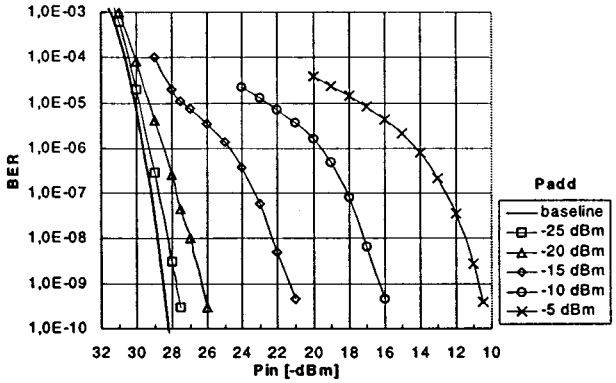

Fig. 11. Homo-wavelength crosstalk effect on BER curves for the ADF. ($\lambda_i = \lambda_i' = 1552.52$ nm.)

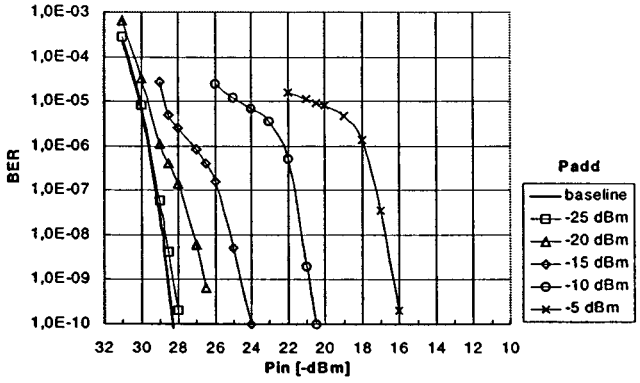

Fig. 12. Homo-wavelength crosstalk effect on BER curves for the ADF with an additional filter after the LE node laser. ($\lambda_i = \lambda_i' = 1552.52$ nm.)

In Fig. 11, BER curves at the LE Rx are reported as functions of the downstream input power, $P_{\text{in}}[\lambda_i]$, and of the upstream added power, $P_{\text{add}}[\lambda_i']$, at the related ADF ports.

The measurement confirmed that this kind of crosstalk is the cause of the main penalty effect when the received power is well above the receiver sensitivity. The penalty increases with increasing P_{add} because, given a value of P_{in}, this implies the increase of ΔP_{ho} and the impairment of SCR_{ho}, see, (1). Nevertheless, a low BER (e.g., 10^{-9} as a reference level) can be achieved independently on absolute power levels when ΔP_{ho} is lower than 6 dB. A qualitative interpretation of these measurements is proposed. From the isolation value ($X_{ho} = 15$ dB) measured at $\lambda = 1552.5$ nm, SCR_{ho} is calculated to be 9 dB. This value is higher than the one expected for noncoherent interference, but smaller than the one required in the case of perfectly coherent crosstalk [5]. Thus, the partially coherent nature of this kind of crosstalk seems to be confirmed by the actual slight mismatch between the wavelengths of interfering channels, causing an incomplete overlapping of their spectra.

As outlined in Section II-B, a system countermeasure against homo-wavelength crosstalk is to lower the power level of the added channel. However, the minimum transmitted power must obey the constraints imposed by the ring power budget, so that it is not always possible to solve the problem merely by adopting this solution. Another countermeasure is the improvement of the isolation X_{ho}. It has been verified, however, that this solution by itself, although helpful, is not satisfactory either. Some tests have been carried out using for comparison a commercial Bragg grating-based device. Although characterized by good isolation ($X_{ho} = 28$ dB), its use led to a negligible penalty reduction.

The cause of this effect has been identified in the intrinsic "notch" nature of the ADF "bar" spectral response. Only the main peak of the spectrum of the laser transmitting to the add port is filtered out, whereas the spectrum parts that fall outside the ADF notch, including sidelobes, reach the drop port without being attenuated. Their impact is unexpectedly relevant, in spite of the use of lasers with a side-mode suppression ratio better than 40 dB. This interpretation is supported by further measurements carried out by placing an additional Fabry–Perot filter just before the add port to clean the laser spectrum. The remarkably improved BER curves obtained are shown in Fig. 12.

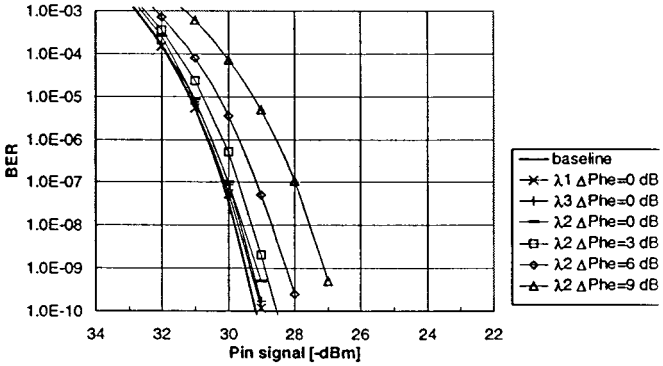

Fig. 13. Hetero-wavelength crosstalk effect on BER curves for the ADF. Crosstalk generated by a single channel. ($\lambda_i = 1546.12$ nm, $\lambda_1 = 1549.32$ nm, $\lambda_2 = 1552.52$ nm, $\lambda_3 = 1555.75$ nm.)

The ADF hetero-wavelength crosstalk performances were evaluated on a different setup of the test bench shown in Fig. 10 by dropping the channel λ_i in the presence of other channels λ_k (where $k \neq i$) passing through the device; the added channel at λ_i' is not present in this case.

In Fig. 13, BER curves are reported as a function of the WDM input power to the ADF, $P_{\text{in}}[\lambda_i]$ under different conditions. The crosstalk interference is generated by a single channel transmitted at different wavelengths. The three curves close to the baseline are related to a power level of the interfering channel equal to the power level of the signal channel (i.e., $\Delta P_{he} = 0$ dB). Under these conditions, no significant penalties are noted when the wavelength of the disturbing channel is changed. The slight relative shift of the curves is due to the different depth of the notches of the ADF "cross" function. The other three curves are obtained for different values of ΔP_{he} when the worst interfering channel is chosen. The curve shifts in this case are more marked because the effect of a power imbalance between channels is important, as noted in Section II-B. The main result deduced from Fig. 13 is that the realized component, characterized by an X_{he} value of around 18 dB, ensures satisfactory performance for the four-wavelength ring for which it was developed. In fact, the penalty due to the hetero-wavelength crosstalk is lower than 1 dB, provided that ΔP_{he} is equal to or lower than 6 dB.

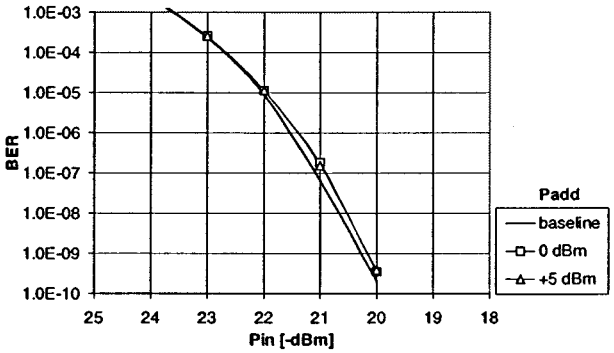

Fig. 14. Homo-wavelength crosstalk effect on BER curves for the AADF. Modulating bit rate: 1.06 Gb/s.

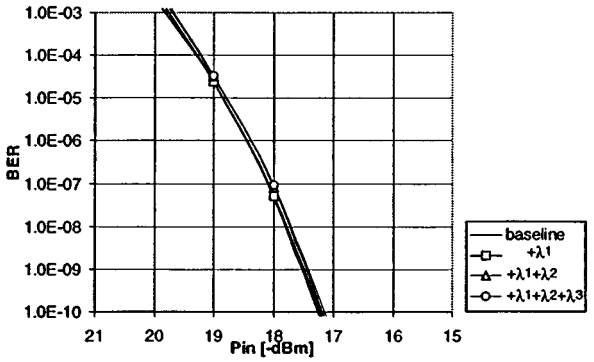

Fig. 15. Hetero-wavelength crosstalk effect on BER curves for the AADF. Channels are modulated at 1.06 Gb/s with different pattern. ($\lambda_i = 1550.92$ nm, $\lambda_1 = 1546.12$ nm, $\lambda_2 = 1547.72$ nm, $\lambda_3 = 1549.32$ nm.)

Similar measurements have been taken in the case of crosstalk generated by two different channels. Under these conditions, slightly better results are obtained, for equal values of ΔP_{he}. This can be understood by considering the different probabilistic distributions of interfering signals, arising from one and from two (uncorrelated) bit patterns, respectively. It is confirmed that, for equal SCR_{he}, the worst case impact is to be expected when the hetero-wavelength interference is caused by one interfering channel.

B. AADF Characterization

Characterization tests similar to the ones previously outlined for the ADF have also been carried out on the AADF component described in Section V. The peculiar feature of this device is the separation of the add and drop functions. This design ensures a solution to the homo-wavelength crosstalk issue.

The homo-wavelength crosstalk measurements were taken on the test bench presented in Fig. 10, set as described for the corresponding measurements related to the ADF. In Fig. 14, BER curves are sketched as a function of $P_{\mathrm{in}}[\lambda_i]$ for two values of $P_{\mathrm{add}}[\lambda_i']$: 0 dBm, $+5$ dBm. The results show the total absence of penalty at the LE Rx even for $\Delta P_{ho} = 25$ dB, leading to homo-wavelength crosstalk-free behavior. The hetero-wavelength crosstalk measurements have been taken on the test bench shown in Fig. 10. The reference WDM comb consisted of four channels.

Slightly different measurements are shown in this case to provide complementary information related to a realistic network environment. The power of each interfering channel, $P_{\mathrm{in}}[\lambda_k] k \neq i$, is kept at a fixed level (-8 dBm each), while the dropped signal power, $P_{\mathrm{in}}[\lambda_i]$, is varied. Different values of SCR_{he} are obtained in this case by changing the number of interfering channels from one to three. Therefore, parametric BER curves depending on the number of interfering channels, and not on the power imbalance ΔP_{he}, are sketched. The value of ΔP_{he} varies along each curve, and can be calculated, point by point, by subtracting the abscissa $P_{\mathrm{in}}[\lambda_i]$ from the total interfering power characteristic of each curve (-8, -5, and -3.3 dBm for one, two, and three interfering channels, respectively). For example, $P_{\mathrm{in}}[\lambda_i] = -20$ dBm corresponds to $\Delta P_{he} = 12$, 15, and 16.7 dB, respectively. The results are shown in Fig. 15. It can be seen that the penalty caused by hetero-wavelength crosstalk at the LE Rx is negligible even for three interfering channels.

It should be noted that measurements shown in Figs. 14 and 15 were performed by using different receivers, so that the two baseline curves are independent references for the single diagrams, and can not be significantly compared.

A two-node network test bench with four wavelengths (matching the real demonstrator network) has been setup by employing two AADF's. Error-free performance has been observed and four AADF's have been operated successfully in the COBNET field trial over several months.

VIII. Conclusions

The realization of the two types of add–drop filters presented in this paper demonstrates the feasibility of integrated components of this kind, which are suitable to fulfill tunability requirements over a large spectral range. Their successful use in an optical network field trial (within the COBNET project) has pointed out the usefulness as basic elements for low-cost OADM nodes. The system characterization was reported in detail. The effects related to crosstalk generation inside the ADF have been measured and their impact identified, leading to the alternative solution of the AADF structure. This proved to fully eliminate homo-wavelength crosstalk. In the BER measurements also no power penalty was observed for hetero-wavelength crosstalk.

References

[1] G. R. Hill *et al.*, "A transport network layer based on optical network elements," *J. Lightwave Technol.*, vol. 11, pp. 667–679, May 1993.

[2] C. Brackett, "Is there an emerging consensus on WDM networking?," *J. Lightwave Technol.*, vol. 14, pp. 936–941, June 1996.

[3] J. M. Simmons, E. L. Goldstein, and A. M. Saleh, "Quantifying the benefit of wavelength add-drop in WDM rings with distance independent and dependent traffic," *J. Lightwave Technol.*, vol. 17, pp. 48–57, Jan. 1996.

[4] W. Denzel and B. Meekers, "Photonics in the backbone of corporate networks—The ACTS COBNET project," in *Proc. NOC'97*. Antwerp, Belgium, 1997, pp. 225–232.

[5] T. Mizuochi, T. Kitayama, K. Shimizu, and K. Ito, "Interferometric crosstalk-free optical add/drop multiplexer using Mach–Zehnder-based fiber gratings," *J. Lightwave Technol.*, vol. 16, pp. 265–276, Feb. 1998.

[6] D. A. Smith, R. S. Chakravarthy, Z. Bao, J. E. Baran, J. L. Jackel, A. d'Alessandro, D. J. Frtiz, S. H. Huang, X. Y. Zou, S. M. Hwang, A. E. Willner, and K. D. Li, "Evolution of the acousto-optic wavelength routing switch," *J. Lightwave Technol.*, vol. 14, pp. 1005–1019, 1996.

[7] H. Hermann, K. Schäfer, and C. Schmidt, "Low-loss tunable integrated acoustooptical wavelength filter in $LiNbO_3$ with strong sidelobe suppression," *IEEE Photon. Technol. Lett.*, vol. 10, pp. 120–122, 1998.
[8] M. Kuznetsov, "Cascaded coupler Mach–Zehnder channel dropping filter for wavelength division multiplexed optical systems," *J. Lightwave Technol.*, vol. 12, pp. 226–230, 1994.
[9] K. Jinguji and M. Kawachi, "Synthesis of coherent two-port lattice form optical delay-line circuits," *J. Lightwave Technol.*, vol. 13, pp. 73–82, Jan. 1995.
[10] D. Di Mola, M. Lenzi, G. Sanvito, E. Fioravanti, and G. Anzalone, "FIR lattice flat-band add/drop filter design," in *Proc. WFOPC*, Sept. 1998.
[11] D. Di Mola and S. Brunazzi, "Tunable optical waveguide add/drop filter for multi-wavelength applications," in *Proc. ECIO'97*, Apr. 1997, paper EFE4-1, pp. 582–585.
[12] H. H. Yaffe, C. H. Henry, M. R. Serbin, and L. G. Cohen, "Resonant couplers acting as add/drop filters made with silica on silicon waveguide technology," *J. Lightwave Technol.*, vol. 12, pp. 1010–1014, 1994.
[13] D. Di Mola, M. Lenzi, A. Carrera, S. Rotolo, S. Brunazzi, and A. Tanzi, "Tunable add/drop filter in LPCVD glass-on-silicon technology for OADM-based ring networks," in *Proc. ECOC'98*, vol. 1, Madrid, Spain, 1998, pp. 123–124.
[14] D. Di Mola, L. Brioschi, A. Carrera, F. Fusari, M. Lenzi, and G. Ongaro, "Unstressed nickel chromium thin films for thermo-optic application," in *Proc. COMMAD'98*, 1998.
[15] G. L. Bona, W. E. Denzel, B. J. Offrein, R. Germann, H. W. M. Salemink, and F. Horst, "Wavelength division multiplexed add/drop ring technology in corporate backbone networks," *Opt. Eng.*, vol. 37, no. 12, pp. 3218–3228, 1998.
[16] B. J. Offrein, G. L. Bona, F. Horst, H. W. M. Salemink, R. Beyeler, and R. Germann, "Wavelength tunable optical add-after-drop filter with flat passband for WDM networks," *IEEE Photon. Technol. Lett.*, vol. 11, no. 2, pp. 239–241, 1999.
[17] M. M. Spühler, B. J. Offrein, G.-L. Bona, R. Germann, I. Massarek, and D. Erni, "A very short planar silica spot-size converter using a nonperiodic segmented waveguide," *J. Lightwave Technol.*, vol. 16, pp. 1680–1685, 1998.
[18] B. J. Offrein, R. Germann, F. Horst, H. W. M. Salemink, R. Beyeler, and G. L. Bona, "Resonant coupler-based tunable add-after-drop filter in silicon-oxynitride technology for WDM networks," *IEEE J. Select. Top. Quantum Electron.: Special Issue on Fiber-Optic Passive Components*, vol. 5, pp. 1400–1406, 1999.
[19] B. J. Offrein, F. Horst, G. L. Bona, H. W. M. Salemink, R. Germann, and R. Beyeler, "Wavelength tunable 1-from-16 and flat passband 1-from-8 add-drop filters," *IEEE Photon. Technol. Lett.*, vol. 11, pp. 1440–1442, 1999.

Salvatore Rotolo received the Doctorate degree in electronic engineering from Politecnico di Milano, Italy, in 1981.

Since then he has been involved in fiber-optic transmission systems. He has been leading the Italtel Project teams in RACE and ACTS Projects in the area of advanced optical broad-band networks (R1012, BLNT; R2028, MWTN; AC029, WOTAN; AC069, COBNET; AC231, MOON). Presently, with the 'Central Research' of Siemens Information and Communication Networks S.p.A, he is heading the "Exploratory Development" Laboratory. He is regularly attending and contributing to ETSI and ITU Standardisation activities. He has been the coauthor of several publications on fiber-optic systems and optical networking.

Alberto Tanzi (M'95) received the Doctor degree in electronic engineering at Politecnico di Milano, Italy, in 1994.

In the same year, he joined the Optical System Group, Central R&D Department at Italtel S.p.a., Milan, Italy, where his work was focused on design and integration of optical systems, and on study and simulation of WDM optical networks. In June 1999, he joined the Optical Networking Group, R&D Department at Pirelli Optical Systems (now Cisco Photonics Italy S.r.l.), Milano, Italy, where he is currently working on optical protection strategies and OADM architectures.

Stefano Brunazzi received the Doctorate degree in electronic and telecommunications engineering from Università di Pavia, Italy, in 1992.

in 1993, he joined Italtel, Central R&D Department, where he has been involved in research activities on WDM systems and optical networking, mainly in the context of European projects (RACE, ACTS, now IST). He is currently with Siemens Information and Communication Networks S.p.A (Milano), Central Research, Exploratory Development Lab, where his activity is focused on the architectures of photonic systems and on the design strategies for optical transport networks. He has been a coauthor of several papers in the areas of optical systems and networking.

Domenico DiMola (M'99) received the Doctorate degree in electronic engineering from Politecnico di Torino, Italy, in 1992. In 1994, he received the "G. Anelli Proficiency post-graduate diploma," in thermodynamics at Politecnico di Torino, Italy.

in 1995, he joined Italtel R&D, where he has been involved in research activities on WDM photonic technologies. He is currently with Gefran S.p.A (Provaglio d'Iseo — Brescia, Italy), where he is responsible of business development in Microsystems technologies Division.

Dr. DiMola is member of the IEEE Lasers and Electro-Optics Society (LEOS)

Lucio Cibinetto received the diploma degree in telecommunications from the Istituto Majorana, Italy, in 1984.

In 1987, he joined the Optoelectronic Group at Alcatel Telettra, Vimercate, Italy, as an Optoelectronic Modules Designer. In 1993, he joined the Photonic Unit, Central R&D Department at Italtel S.p.a., Milano, Italy, where he works mainly on packaging development of optical passive components. Currently, he his responsible for the optoelectronics devices packaging activities in Italtel.

Maurizio Lenzi (M'99) received the Dr. Ing. degree in electronic engineering from the Politecnico di Torino, Italy, in 1991.

He became Researcher in the "New technology" Laboratory of the Central Research Department of Italtel S.p.A., Italy, where his research was focused on the design of integrated optics devices for telecommunications applications. He is currently with Optowave, a recently founded company, as Product Development Manager for passive integrated optics device. His current activities are focused on the development of integrated optics device like AGW's and VCOA's.

Dr. Lenzi is member of the IEEE Lasers and Electro-Optics Society (LEOS) and the Optical Society of America (OSA).

Gian-Luca Bona received the Ph.D. degree in physics from the Swiss Federal Institute of Technology (ETH), Switzerland, in 1987, for his work on short-pulsed laser excited photoemission.

After Postdoctoral work at the IBM Zurich Research Laboratory, Switzerland, in the area of picosecond optical sampling of ultrafast devices, he became Research Staff Member in 1988, and was involved in work on quantum-well semiconductor lasers, with emphasis on the design and characterization of high-power and short-wavelength GaAs-based lasers. Since 1994, he has been working on low-cost planar waveguide components mainly for wavelength-division-multiplexed applications. He currently manages the IBM research photonic networking effort.

Bert Jan Offrein received the Ph.D. degree in applied physics from the University of Twente, The Netherlands, in 1994. His dissertation examined the measurement of optical nonlinearities and the design and realisation of an all-optical switching device.

From 1995 to 1999, he was with the Optical Networking Group of the IBM Zurich Research Laboratory working on the design and characterisation of optical components for DWDM networks. In 1999, he joined JDS Uniphase.

Folkert Horst received the M.S. degree in applied physics and the Ph.D. degree in electronics engineering from the University of Twente, Enschede, The Netherlands, in 1992 and 1997, respectively.

In 1997, he joined the Optical Networking Group of the IBM Zurich Research Laboratory, Rüschlikon, Switzerland. His current research involves the design and characterization of components for DWDM optical networks based on SiON technology.

Roland Germann received the Ph.D. degree in physics from the University of Stuttgart, Germany, in 1990. His dissertation deals with dry etching of III–V semiconductors for the fabrication of nanostructures and DFB lasers as well as the optical and electrical characterization of dry-etch-induced damage.

In 1990, he joined the IBM Zurich Research Laboratory, Switzerland, as a Research Staff Member, working on the fabrication technology of semiconductor lasers for optical data communication and storage applications. His current work is focused on the development of SiON-based optical waveguide devices for WDM networks.

Dr. Germann is a member of the German Physical Society.

Huub W. M. Salemink received the Ph.D. degree in superconductivity from Nijmegen University, The Netherlands, in 1973.

He has worked on research topics in optical applications in the fields of semiconductor lasers and remote sensing. He joined the IBM Zurich Research Laboratory, Switzerland, as a Research Staff Member in 1985, where he has worked on the application of tunneling microscopy to study dopant distributions as well as to analyze semiconductor interfaces and III–V alloys at the atomic scale. Currently, he is engaged in research on materials aspects of SiON-based compounds used in waveguide fabrication. Since 1996, he has also served as Visiting Professor of the Foundation Physica at the Technical University of Delft, The Netherlands.

Peter H. Baechtold received the Swiss Federal Technician diploma in electronics and telecommunication in 1970.

After working several years abroad, mainly in the telecom and instrumentation business, he joined IBM in 1977. There he developed one of the first 12–bit signal processors, in those days a 19" rack full of electronic components, used for early modem applications. Currently, he is involved in testing and qualifying SDH/SONET framer chips and developing an add–drop digital cross-connect multiplexer application.